PERGAMON

International Journal of Solids and Structures 38 (2001) 3021–3037

INTERNATIONAL JOURNAL OF SOLIDS and STRUCTURES

www.elsevier.com/locate/ijsolstr

Transient waves in a functionally graded cylinder

X. Han, G.R. Liu *, Z.C. Xi, K.Y. Lam

Department of Mechanical and Production Engineering, National University of Singapore, 10 Kent Ridge Crescent, Singapore 119260, Singapore

Received 13 October 1999; in revised form 15 December 1999

Abstract

A hybrid numerical method (HNM) is presented for analyzing transient waves in a cylinder made of functionally graded material (FGM). In the HNM, the FGM cylinder is divided into N cylindrical elements with three-nodal line in the wall thickness. The elemental material properties are assumed to vary linearly in the thickness direction to better model the spatial variation of material properties of FGM. The Hamilton variational principle is used to develop governing equations of the cylinder. The displacement responses are determined by employing the Fourier transformations together with the modal analysis. The HNM is applied to analyze a number of FGM cylinders, and its efficiency is demonstrated.

Keywords: Graded cylinder; Transient waves; Hybrid numerical method

1. Introduction

The mechanical properties of cylindrical structures made of functionally graded material (FGM) vary continuously in the macroscopic sense from one surface to the other. This is achieved by gradually varying the volume fraction of the constituent materials in the manufacturing process. The advantage of FGMs is that they are able to withstand high-temperature-gradient environments while maintaining their structural integrity. In the application of FGM cylindrical structures to aerospace, nuclear and automobile industries, analyses of transient waves in FGM cylinders are of great importance.

There have been many works on wave propagation problems related to composite cylindrical shells. Mirsky (1964) and Nowwinski (1967) solved for axially symmetric waves in orthotropic shells. Chou and Achenbach (1981) provided a three-dimensional solution for orthotropic shells as well. Yuan and Hsieh (1998) proposed an analytical method for the investigation of free harmonic wave propagation in laminated shells. Nayfeh (1995) discussed scattering of horizontally polarized elastic waves from multilayered anisotropic cylinders embedded in isotropic solids. However, studies on the transient responses of FGM shells have not been found in the literature.

* Corresponding author. Tel.: +65-874-6481; fax: 65-779-1459.
E-mail address: mpeliugr@nus.edu.sg (G.R. Liu).

0020-7683/01/$ - see front matter
PII: S0020-7683(00)00219-5

As the material properties of FGM change with the structural thickness, wave propagation problems related to the FGM are generally difficult to analyze without resorting to numerical approaches. There have been methods proposed for wave propagation problems of FGM plates. Liu et al. (1991a) and Liu and Tani (1992) used strip element method to deal with an FGM plate. Ohyoshi et al. (1996) proposed an analytical method and obtained wave reflection and transmission coefficients for an FGM plate. Recently, Liu et al. (1999a) proposed a method for analyzing stress waves in FGM plates. The results show that the variation of material properties can be approximated with piecewise linear functions.

This paper presents a hybrid numerical method (HNM), which combines the finite element method with the Fourier transformation method. The concept of the HNM was originally proposed by Liu et al. (1991b) for treating transient waves in anisotropic laminated plates. The HNM concept is extended in this paper to cylinders made of FGM. In the HNM, the FGM cylinder is divided into layered cylindrical elements in the thickness direction. The HNM is also formulated to accommodate a linear variation of material properties in an element in the thickness direction. The Hamilton variational principle is used to develop governing equations of the cylinder. The displacement response is determined by employing the Fourier transformations and the modal analysis. The HNM can reduce the number of elements and obtain more accurate results. This method is applied to a number of FGM cylinders. First, the displacement responses of a SiC–C plate are computed and the results are compared with those obtained by existing methods. Next, the displacement responses of FGM cylinders excited by an incident wave of one cycle of sine function are calculated, and some interesting results are obtained.

2. Formulation

Consider an FGM cylinder with varying material properties in the thickness direction. The thickness, inner radius and outer radius of the cylinder are denoted by H, R_1, R_2, respectively, as shown in Fig. 1. Let x and z denote, respectively, the axial and radial coordinates. The cylinder is subjected to a radial line load of $q = q_0\delta(x)f(t)$ uniformly distributed along the circumferential direction, where δ is the Dirac delta function, and $f(t)$ is a function of the time. Because the geometry of the cylinder and the load are independent of the circumferential direction, the problem is axisymmetric.

In the case of axisymmetry, the strain–displacement relations are given by

$$\boldsymbol{\varepsilon} = \mathbf{L}\mathbf{U}, \tag{1}$$

where $\boldsymbol{\varepsilon} = [\,\varepsilon_x \quad \varepsilon_\theta \quad \varepsilon_z \quad \varepsilon_{xz}\,]^{\mathrm{T}}$ is the vector of strains, $\mathbf{U} = [\,u \quad w\,]^{\mathrm{T}}$ is the vector of displacements, u and w are the displacements in the axial and radial directions, respectively, and $\mathbf{L}$ is the operator matrix given by

$$\mathbf{L} = \begin{bmatrix} \frac{\partial}{\partial x} & 0 & 0 & \frac{\partial}{\partial z} \\ 0 & \frac{1}{R_1+z} & \frac{\partial}{\partial z} & \frac{\partial}{\partial x} \end{bmatrix}^{\mathrm{T}}. \tag{2}$$

The operator matrix $\mathbf{L}$ can be rewritten as

$$\mathbf{L} = \mathbf{L}_1\frac{\partial}{\partial x} + \mathbf{L}_2\frac{\partial}{\partial z} + \mathbf{L}_3\frac{1}{R_1+z} = \begin{bmatrix} 1 & 0 \\ 0 & 0 \\ 0 & 0 \\ 0 & 1 \end{bmatrix}\frac{\partial}{\partial x} + \begin{bmatrix} 0 & 0 \\ 0 & 0 \\ 0 & 1 \\ 1 & 0 \end{bmatrix}\frac{\partial}{\partial z} + \begin{bmatrix} 0 & 0 \\ 0 & 1 \\ 0 & 0 \\ 0 & 0 \end{bmatrix}\frac{1}{R_1+z}, \tag{3}$$

where the radial coordinate is decomposed as $R_1 + z$. It is assumed that the material is transversely isotropic, and the stresses are related to strains by

$$\boldsymbol{\sigma} = \mathbf{c}\boldsymbol{\varepsilon}, \tag{4}$$

where $\boldsymbol{\sigma} = [\,\sigma_x \quad \sigma_\theta \quad \sigma_z \quad \sigma_{xz}\,]^{\mathrm{T}}$ is the vector of stresses and $\mathbf{c}$ is the matrix of material constants given as

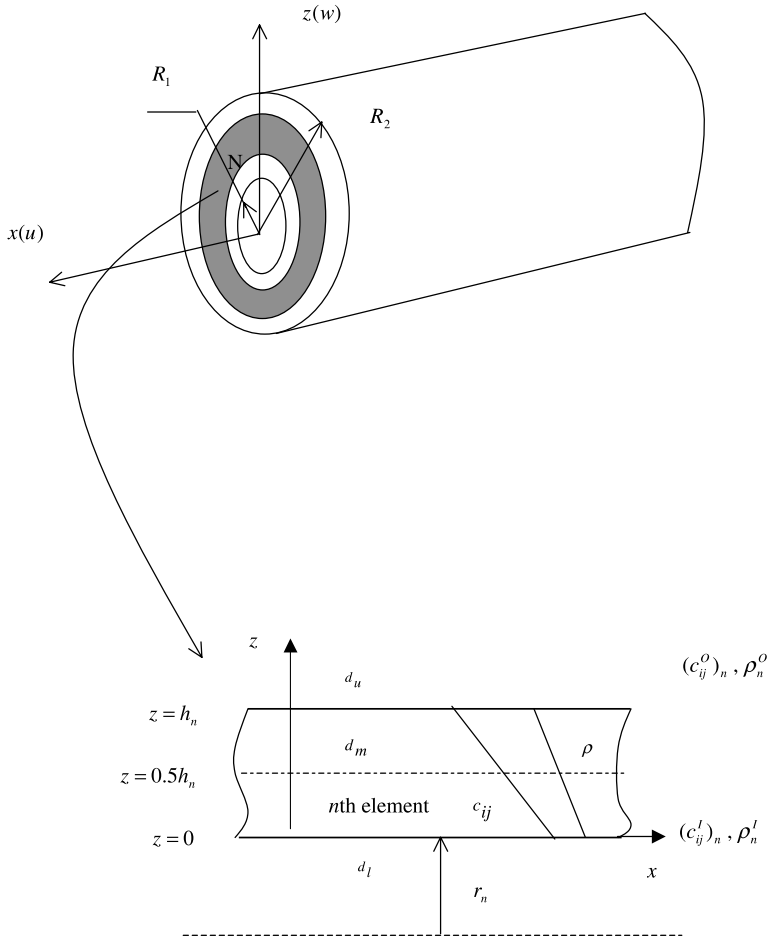

Fig. 1. An FGM cylinder and its nth isolated element.

$$\mathbf{c} = \begin{bmatrix} c_{11} & c_{12} & c_{13} & 0 \\ & c_{22} & c_{23} & 0 \\ & & c_{33} & 0 \\ \text{sym} & 0 & 0 & c_{44} \end{bmatrix}. \tag{5}$$

The stresses acting on a surface can be written as

$$\mathbf{R}_z = \mathbf{L}_2^{\mathrm{T}}\mathbf{c}\mathbf{L}\mathbf{U}. \tag{6}$$

Finally, the initial conditions of the cylinder are given by

$$\mathbf{U}|_{t=0} = \dot{\mathbf{U}}|_{t=0} = 0, \tag{7}$$

where "·" represents the differentiation with respect to time.

The cylinder is divided into N layered cylindrical elements. The thickness and inner radius of the nth element are denoted by h_n and r_n, respectively. It can be found that the outer radius of the nth element is equal to $r_n + h_n$. The elastic coefficient matrix and the mass density on the inner and outer surfaces of the nth element are denoted by $c_n^{\mathrm{I}} = (c_{ij})_n^{\mathrm{I}}$ $(i, j = 1, 2, 3, 4)$, ρ_n^{I}, $c_n^{\mathrm{O}} = (c_{ij})_n^{\mathrm{O}}$ $(i, j = 1, 2, 3, 4)$ and ρ_n^{O} respectively,

as shown in Fig. 1, where the superscripts 'I' and 'O' respect the inner and outer surface, respectively. It is assumed that the material properties of the nth element change linearly in the thickness direction:

$$c_n = (c_n^{\mathrm{O}} - c_n^{\mathrm{I}})\frac{z}{h_n} + c_n^{\mathrm{I}} = \Delta c_{ij}^n \bar{z} + (c_{ij}^{\mathrm{I}})_n, \tag{8}$$

$$\rho_n = (\rho_n^{\mathrm{O}} - \rho_n^{\mathrm{I}})\frac{z}{h_n} + \rho_n^{\mathrm{I}} = \Delta \rho_n \bar{z} + \rho_n^{\mathrm{I}}. \tag{9}$$

We approximate the displacement field within an element as

$$\mathbf{U} = \mathbf{N}\mathbf{d}, \tag{10}$$

where $\mathbf{N}$ is the shape function matrix of second order given by

$$\mathbf{N} = [(1 - 3\bar{z} + 2\bar{z}^2)\mathbf{E}\, 4(\bar{z} - \bar{z}^2)\mathbf{E}(2\bar{z}^2 - \bar{z})\mathbf{E}]. \tag{11}$$

Here, $\mathbf{E}$ is a 2×2 identity matrix and $\bar{z} = z/h_n$, and $\mathbf{d}$ is the displacement amplitude vector at $z = 0$, $z = 0.5h_n$ and $z = h_n$ as follows:

$$\mathbf{d} = \begin{bmatrix} d_l^{\mathrm{T}} & d_m^{\mathrm{T}} & d_n^{\mathrm{T}} \end{bmatrix}^{\mathrm{T}}. \tag{12}$$

A governing equation of the element follows from the Hamilton variational principle, which takes the form

$$\int_{t_0}^{t_1} \delta(V - T)\mathrm{d}t = 0. \tag{13}$$

Here, the time t_0 and t_1 are arbitrary, V and T are the potential energy and kinetic energy of the element, respectively. The potential energy of the element in the absence of body force is given by

$$V = \pi \int_0^{h_n} \boldsymbol{\varepsilon}^{\mathrm{T}} \boldsymbol{\sigma}(r + z)\mathrm{d}z - 2\pi w q R_2. \tag{14}$$

The kinetic energy of the element is expressed in terms of the displacement vector as

$$T = \pi \int_0^{h_n} \frac{\partial \mathbf{U}^{\mathrm{T}}}{\partial t}\frac{\partial \mathbf{U}}{\partial t}\rho(r + z)\mathrm{d}z. \tag{15}$$

Substituting Eqs. (14) and (15) into Eq. (13), and taking variation with respect to $\mathbf{U}$ leads to the following governing ordinary differential equations of the element:

$$\mathbf{q} = \mathbf{M}'\ddot{\mathbf{d}} + \mathbf{K}_{\mathbf{D}}\mathbf{d}, \tag{16}$$

where the dot represents the derivative with respect to the time, and

$$\mathbf{K}_{\mathbf{D}} = -\mathbf{B}_2\frac{\mathrm{d}^2}{\mathrm{d}x^2} + \mathbf{B}_1\frac{\mathrm{d}}{\mathrm{d}x} + \mathbf{B}_0. \tag{17}$$

The subscript '**D**' denotes that $\mathbf{K}$ is a differential operator matrix, and

$$\mathbf{B}_2 = \mathbf{A}_2 + \mathbf{A}_2^{\mathrm{d}}, \tag{18}$$

$$\mathbf{B}_1 = \mathbf{A}_1 + \mathbf{A}_1^{\mathrm{d}}, \tag{19}$$

$$\mathbf{B}_0 = \mathbf{A}_0 + \mathbf{A}_0^{\mathrm{d}}, \tag{20}$$

$$\mathbf{M}' = \mathbf{M} + \mathbf{M}_{\mathrm{d}}. \tag{21}$$

The matrices $\mathbf{A}_i$ $(i = 0, 1, 2)$, $\mathbf{M}$ and $\mathbf{q}$ are given by Xi et al. (1999), if the density and the elastic coefficients on the inner surface of the element are used as constants. The matrices $\mathbf{M}_\mathrm{d}$ and $\mathbf{A}_i^\mathrm{d}$ $(i = 0, 1, 2)$ are the additional matrices for the variation of the density and the elastic coefficients in the elemental thickness direction, and are given by

$$\mathbf{A}_0^\mathrm{d} = \int_0^{h_n} \left[\frac{\partial \mathbf{N}^\mathrm{T}}{\partial z} \mathbf{D}_3' \frac{\partial \mathbf{N}}{\partial z} (r_n + z)z + \left(\mathbf{N}^\mathrm{T} \frac{\partial \mathbf{N}}{\partial z} + \frac{\partial \mathbf{N}^\mathrm{T}}{\partial z} \mathbf{N} \right) z \mathbf{D}_5' + \mathbf{N}^\mathrm{T} \mathbf{D}_6' \mathbf{N} \frac{z}{r_n + z} \right] \mathrm{d}z, \tag{22}$$

$$\mathbf{A}_1^\mathrm{d} = \int_0^{h_n} \left[\left(2 \frac{\partial \mathbf{N}^\mathrm{T}}{\partial z} \mathbf{D}_2'' \mathbf{N} - \frac{\partial \mathbf{N}^\mathrm{T}}{\partial z} \mathbf{D}_2''' \mathbf{N} - \mathbf{N}^\mathrm{T} \mathbf{D}_2''' \frac{\partial \mathbf{N}}{\partial z} \right) (r_n + z)z + 2\mathbf{N}^\mathrm{T} \mathbf{D}_4'' \mathbf{N} z - 2\mathbf{N}^\mathrm{T} \mathbf{D}_4''' \mathbf{N} z \right] \mathrm{d}z, \tag{23}$$

$$\mathbf{A}_2^\mathrm{d} = \int_0^{h_n} \mathbf{N}^\mathrm{T} \mathbf{D}_1' \mathbf{N} (r_n + z) z \, \mathrm{d}z, \tag{24}$$

$$\mathbf{M}^\mathrm{d} = \int_0^{h_n} \mathbf{N}^\mathrm{T} \Delta\rho_n \mathbf{N} (r + z) z \, \mathrm{d}z. \tag{25}$$

The expressions for matrices $\mathbf{A}_i^\mathrm{d}$ $(i = 1, 2)$, $\mathbf{M}_\mathrm{d}$ and $\mathbf{D}_3'$, $\mathbf{D}_5'$, $\mathbf{D}_6'$, $\mathbf{D}_1'$, $\mathbf{D}_2''$, $\mathbf{D}_4''$, $\mathbf{D}_2'''$, $\mathbf{D}_4'''$ are given in Appendix. As can be seen from Eq. (16), the original partial differential equations of the cylinder with three variables (x, y, t) have simplified to a system of ordinary differential equations by the above procedure.

Assembling all the elements, a system of approximate differential equations for the whole cylinder may be expressed as

$$\mathbf{q}_\mathrm{t} = \mathbf{M}_\mathrm{t} \ddot{\mathbf{d}}_\mathrm{t} + \mathbf{K}_{\mathbf{D}_\mathrm{t}} \mathbf{d}_\mathrm{t}, \tag{26}$$

where

$$\mathbf{K}_{\mathbf{D}_\mathrm{t}} = -\mathbf{B}_{2\mathrm{t}} \frac{\mathrm{d}^2}{\mathrm{d}x^2} + \mathbf{B}_{1\mathrm{t}} \frac{\mathrm{d}}{\mathrm{d}x} + \mathbf{B}_{0\mathrm{t}}. \tag{27}$$

In these equations, the subscript 't' denotes matrices or vectors for the whole cylinder. The matrices $\mathbf{B}_{i\mathrm{t}}$ $(i = 0, 1, 2)$, $\mathbf{M}_\mathrm{t}$ and the vectors $\mathbf{q}_\mathrm{t}$ and $\mathbf{d}_\mathrm{t}$ can be obtained by assembling the corresponding matrices and vectors of adjacent elements. The sizes of $\mathbf{d}_\mathrm{t}$ and $\mathbf{q}_\mathrm{t}$ are $M \times 1$, and the sizes of the matrices $\mathbf{M}_\mathrm{t}$ and $\mathbf{B}_{i\mathrm{t}}$ are $M \times M$, where $M = 2(2N + 1)$.

We introduce the Fourier transformations with respect to the axial coordinate x in the form

$$\tilde{\mathbf{d}}(k, t) = \int_{-\infty}^{+\infty} \mathbf{d}(x, t) \mathrm{e}^{\mathrm{i}kx} \, \mathrm{d}x, \tag{28}$$

where $i = \sqrt{-1}$, and the real transformation parameter k is the wave number corresponding to the axial coordinate x. The application of the Fourier transformations indicated by Eqs. (26)–(28) leads to

$$\tilde{\mathbf{q}}_\mathrm{t} = \mathbf{M}_\mathrm{t} \ddot{\tilde{\mathbf{d}}}_\mathrm{t} + \mathbf{K}_\mathrm{t} \tilde{\mathbf{d}}_\mathrm{t}, \tag{29}$$

where $\tilde{\mathbf{d}}$ and $\tilde{\mathbf{q}}_\mathrm{t}$ are the Fourier transformations of $\mathbf{d}$ and $\mathbf{q}_\mathrm{t}$, respectively, and $\mathbf{K}_\mathrm{t}$ is the stiffness matrix given by

$$\mathbf{K}_\mathrm{t} = k^2 \mathbf{B}_{2\mathrm{t}} + \mathrm{i}k \mathbf{B}_{1\mathrm{t}} + \mathbf{B}_{0\mathrm{t}}. \tag{30}$$

From Appendix and the work of Xi et al. (1999), we can see that $\mathbf{M}_\mathrm{t}$, $\mathbf{B}_{2\mathrm{t}}$, $\mathbf{B}_{0\mathrm{t}}$ are symmetric, and $\mathbf{B}_{1\mathrm{t}}$ is antisymmetric. Hence $\mathbf{K}_\mathrm{t}$ is a Hermitian matrix typically.

The modal analysis is used to obtain the Fourier transformation of the displacement vector. Solving the following eigenvalue equation corresponding to Eq. (29),

$$0 = [\mathbf{K}_t - \omega^2 \mathbf{M}_t]\phi^R, \tag{31}$$

we can get the eigenfrequencies ω_m $(m = 1, 2, 3 \ldots M)$ and the corresponding right eigenvectors ϕ_m^R. For a time-step impact load, we can give the displacement in the Fourier transformation domain following the method given by Liu et al. (1991b):

$$\tilde{\mathbf{d}}_t(k,t) = \sum_{m=1}^{M} \frac{\varphi_m^L \tilde{\mathbf{q}}_t \varphi_m^R (1 - \cos \omega_m t)}{\omega_m^2 M_m}, \tag{32}$$

where ω_m, φ_m^R and φ_m^L are the mth eigenfrequency and the corresponding right and left eigenvectors, and

$$M_m = \phi_m^L M_t \phi_m^R. \tag{33}$$

Taking the inverse Fourier transformation, the displacement response in the space-time domain can be expressed by

$$\mathbf{d}_t(x,t) = \frac{1}{2\pi} \int_{-\infty}^{+\infty} \tilde{\mathbf{d}}_t(k,t) e^{-ikx} \, dk. \tag{34}$$

The integration in Eq. (34) can be carried out by using the fast Fourier transform (FFT) techniques (Liu et al., 1991b; Liu and Tani, 1994; Liu and Lam, 1999c). Techniques (Liu et al., 1995, 1997) for treating wave field in a laminated composite are here used to improve the efficiency in calculating the displacement response.

3. Material properties of functionally graded material cylinder

Generally, a mixture of ceramic and metal is used to produce FGM. The property of the combined materials can be expressed as

$$P_F(T,z) = \sum_i P_{mi}(T) V_{mi}(z), \tag{35}$$

where P_F is the effective material property of the FGM, P_{mi}, the temperature-dependent property of the ith material, V_{mi}, the volume fraction of the ith material, z, the coordinate in the thickness direction and T, the temperature. The FGM is often used in high-temperature environment and may possess temperature-dependent properties. The property for each material $P_{mi}(T)$ in Eq. (35) can, therefore, be expressed in the form of (Touloukian, 1967)

$$P_{mi}(T) = p_0 \left(\frac{p_{-1}}{T} + 1 + p_1 T + p_2 T^2 + p_3 T^3 \right), \tag{36}$$

where p_0 is the constant appearing in the cubic fit of the material property with temperature, and p_{-1}, p_1, p_2, p_3 are the coefficients of T^{-1}, T, T^2, T^3, respectively, obtained after factoring out p_0 from the cubic curve fit of the property. The material properties are expressed in this way so that the higher order effects of the temperature on material properties would be readily discernible.

The volume fraction $V_{mi}(z)$ is a spatial function and the sum of the volume fractions of all the constituent materials makes 1, i.e.

$$\sum_i V_{mi}(z) = 1. \tag{37}$$

The simple power law exponent of volume fraction distribution is used to provide a measure of the amount of the ith material in the FGM.

For a mixture of two materials at the kth lamina, the effective material property of FGM can be expressed as

$$P_{\mathrm{F}}^{K}(T,z) = P_{m1}^{k}(T)V_{m1}^{k}(z) + P_{m2}^{k}(T)V_{m2}^{k}(z). \tag{38}$$

For the kth lamina containing two constituent materials, Young's modules E_{F}^{k}, Poisson ratio v_{F}^{k} and density ρ_{F}^{k} can be obtained from Eq. (38) as follows:

$$E_{\mathrm{F}}^{k} = E_{1}^{k}V_{1}^{k}(z) + E_{2}^{k}(1 - V_{1}^{k}(z)), \tag{39}$$

$$v_{\mathrm{F}}^{k} = v_{1}^{k}V_{1}^{k}(z) + v_{2}^{k}(1 - V_{1}^{k}(z)), \tag{40}$$

$$\rho_{\mathrm{F}}^{k} = \rho_{1}^{k}V_{1}^{k}(z) + \rho_{2}^{k}(1 - V_{1}^{k}(z)). \tag{41}$$

Four types of FGM cylinders are configured by Gong et al. (1999). They are all composed of stainless steel and silicon nitride. Types 1 and 2 FGM cylinders are single-layer shells. The former has stainless steel on its outer surface and silicon nitride on its inner surface, while the latter has silicon nitride on its outer surface and stainless steel on its inner surface. Types 3 and 4 FGM cylinders are two layers of FGM cylinders. Type 3 has silicon nitride on its outer and inner surfaces and stainless steel on its middle surface. Type 4 has stainless steel on its outer and inner surfaces and silicon nitride on its middle surface. The material properties for stainless steel and silicon nitride are listed in Table 1 (Touloukian, 1967).

For types 1 and 2 FGM cylinders, the volume fraction can be expressed as

$$V_{m1}(z) = \left(\frac{z}{h}\right)^{n}, \quad V_{m2}(z) = 1 - \left(\frac{z}{h}\right)^{n} \quad z \in [0,h], \tag{42}$$

where n is the power law exponent. The value of n is determined by optimization for minimum uniform stress across the thickness. For type 1 FGM cylinder, V_{m1} represents the volume fraction of stainless steel and V_{m2} represents the volume fraction of silicon nitride. For type 2 FGM cylinder, V_{m1} stands for the volume fraction of silicon nitride and V_{m2}, the volume fraction of stainless steel. Thus, the variation of volume fraction for type 2 cylinder with radial position z in the thickness direction is in contrast with that of type 1 FGM cylinder.

For types 3 and 4 FGM cylinders with two layers, the volume fraction can be expressed as

$$V_{\mathrm{m1}}^{1}(z) = \left(\frac{z}{h}\right)^{n}, \quad V_{\mathrm{m2}}^{1}(z) = 1 - \left(\frac{z}{h}\right)^{n} \qquad z \in [0, 0.5h], \tag{43}$$

$$V_{\mathrm{m1}}^{2}(z) = \left(\frac{2z-h}{h}\right)^{n}, \quad V_{m2}^{2}(z) = 1 - \left(\frac{2z-h}{h}\right)^{n} \qquad z \in [0.5h, h]. \tag{44}$$

Table 1
Material properties of stainless steel and silicon nitride FGM (Touloukian, 1967)

Coefficients	Stainless steel			Silicon nitride		
	E (GPa)	v	ρ (kg/m^3)	E (GPa)	v	ρ (kg/m^3)
P_0	201.04	0.3262	8166	348.43	0.24	2370
P_{-1}	0	0	0	0	0	0
P_1	3.079×10^{-13}	-2.002×10^{-4}	0	-3.07×10^{-13}	0	0
P_2	-6.534×10^{-16}	3.97×10^{-7}	0	2.160×10^{-16}	0	0
P_3	0	0	0	-68.946×10^{-20}	0	0
	207.82	0.3177	8166	322.4	0.24	2370

For type 3 FGM cylinder, V_{m1}^k $(k=1,2)$ represents the volume fraction of stainless steel and V_{m2}^k $(k=1,2)$ represents the volume fraction of silicon nitride. For type 4 FGM cylinders, V_{m2}^k $(k=1,2)$ represents the volume fraction of stainless steel and V_{m1}^k $(k=1,2)$ represents the volume fraction of silicon nitride. Therefore, the variations of V_{m1}^k and V_{m2}^k $(k=1,2)$ with radial position z in the thickness direction are opposite to that for type 3 FGM cylinder.

4. Numerical examples

4.1. Computational procedure

First, an FGM cylinder is divided into N elements. For each element, the material constant matrix $\mathbf{c}$ and mass density ρ of surfaces can be obtained by using known functions about the thickness, and matrices $\mathbf{A}_i$, $\mathbf{A}_i^{\mathrm{d}}$, $\mathbf{M}$, $\mathbf{M}_{\mathrm{d}}$ can be obtained as shown in Appendix and the work of Xi et al. (1999). The matrices $\mathbf{M}_{\mathrm{t}}$, $\mathbf{B}_{i\mathrm{t}}$ can be obtained by overlapping the matrices $\mathbf{A}_i$, $\mathbf{A}_i^{\mathrm{d}}$, $\mathbf{M}$, $\mathbf{M}_{\mathrm{d}}$ of the neighboring cylinder elements, in the same way as the finite element method. For a step-impact force, the frequencies and the corresponding left and right eigenvectors can be obtained by solving equation for various wave number k. Using Eq. (32), we can obtain the displacement vector in the Fourier transformation domain. Finally, the displacement response can be obtained by using Eq. (34) and the FFT.

4.2. Calculated results and discussion

In the calculations, the following dimensionless parameters are used:

$$\bar{x}=\frac{x}{H},\qquad \bar{c}_{ij}=\frac{c_{ij}}{c_{44}^{\mathrm{c}}},\qquad \bar{w}=\frac{c_{44}^{\mathrm{c}}w}{q_0R_2},\qquad \bar{u}=\frac{c_{44}^{\mathrm{c}}u}{q_0R_2},\qquad \bar{\omega}=\frac{\omega h}{c_s},\qquad c_s=\sqrt{\frac{c_{44}^{\mathrm{c}}}{\rho_{\mathrm{c}}}},\qquad \bar{r}=\frac{r}{H},$$
$$\bar{\rho}=\frac{\rho}{\rho_{\mathrm{c}}},\qquad t=tc_s/H \tag{45}$$

where c_{44}^{c} and ρ_{c} stand for the reference material constant and mass density. Here, they are equal to the material constant c_{44} and mass density on the inner surface of the cylinder under consideration.

The incident wavelet is assumed to be a radial line load acting on the outer surface of the cylinder. The time history of the incident wavelet is given as

$$f(t)=\begin{cases}\sin(2\pi t/t_{\mathrm{d}}), & 0<t<t_{\mathrm{d}},\\ 0, & t\leqslant 0 \quad\text{and}\quad t\geqslant t_{\mathrm{d}},\end{cases} \tag{46}$$

where t_{d} is the time duration of the incident wavelet and $\omega_f=2\pi/t_{\mathrm{d}}$. In this paper, we set $\bar{t}_{\mathrm{d}}=2$. It means that the wavelet is one cycle of the sine function.

Using the Duhamel integral and viewing Eq. (32), we can get the displacement in the Fourier transformation domain under a sine line load

$$\tilde{\mathbf{d}}_{\mathrm{t}}(k_x,t)=\begin{cases}\displaystyle\sum_{m=1}^{M}\frac{\varphi_m^{\mathrm{L}}\tilde{\mathbf{q}}_{\mathrm{t}}\varphi_m^{\mathrm{R}}(\omega_f\sin(\omega_m t)-\omega_m\sin(\omega_f t))}{\left(\omega_m^2-\omega_f^2\right)M_m\omega_m}, & 0<t\leqslant t_{\mathrm{d}},\\ \displaystyle\sum_{m=1}^{M}\frac{\varphi_m^{\mathrm{L}}\tilde{\mathbf{q}}_{\mathrm{t}}\varphi_m^{\mathrm{R}}\{(\omega_f-\omega_m)\sin[(\omega_f+\omega_m)\tau-\omega_m t]-(\omega_f+\omega_m)\sin[(\omega_f-\omega_m)\tau+\omega_m t]\}|_0^{t_{\mathrm{d}}}}{\varphi_m^{\mathrm{L}}M_m\varphi_m^{\mathrm{R}}\left(\omega_f^2-\omega_m^2\right)\omega_m} & t>t_{\mathrm{d}}\end{cases} \tag{47}$$

To validate the present formulation and numerical implementation, the displacement response on the surface of the SiC–C plate to a sine function line load on the upper surface of the plate is first studied. The

SiC–C plate is made from combining material SiC and C using a chemical vapor deposition technique. The material properties of this plate can be written as a quadratic function of thickness z (Liu et al., 1999b):

$$\bar{E} = A_E + B_E\bar{z} + C_E\bar{z}^2, \tag{48}$$

$$\bar{\rho} = A_\rho + B_\rho\bar{z} + C_\rho\bar{z}^2, \tag{49}$$

where E is Young's modulus and ρ is the mass density of the SiC–C FGM plate. Here, $A_E = 2.62$, $B_E = 0.00$, and $C_E = 28.78$; $A_\rho = 1.80$, $B_\rho = 0.01$ and $C_\rho = 1.42$; $\bar{E} = E/\text{const}$, $\bar{\rho} = \rho/\rho_0$ and const = 9.68 GPa and, $\rho_0 = 1000$ kg/m^3. A comparison of the result provided by the present paper and that previously obtained by Liu et al. (1991b, 1999b) is shown in Fig. 2. A good agreement between these two results is observed. Besides, this example is also used for convergence study to find the number of elements required for analyses. In this case, the present results are obtained with 20 and 25 elements. It can be seen from this figure that with 20 elements, the result is converged to a very good degree of accuracy. Unless otherwise specified, the cylinders are divided into 20 elements radially in the subsequent calculations.

Next, the responses of four types of FGM cylinders are studied. Two ratios of the inner radius to thickness, $R_1/H = 1$ and $R_1/H = 20$, are employed in calculations; the former is viewed as a thick cylinder, whereas the latter is viewed as a cylindrical shell.

Since the square of ω_m is in the denominator of Eq. (47), the value of the fraction decreases rapidly with increasing the order of modes, and very accurate results may be achieved using a few lowest modes in the practical calculation. Fig. 3 shows the time history of the displacement on the outer surface of the type 1 cylindrical shell. The results are obtained using different numbers of modes. It can be seen from this figure that the result obtained using the first eight modes is almost the same as that obtained using the first 14 modes. Therefore, the first eight modes are used in the following calculations.

Figs. 4 and 5 show the time history of the displacement $\bar{u}$ on the outer surface of the type 1 for cylinder and cylindrical shell, respectively. A comparison of the displacement responses between various values of the power law exponent n is presented. It is observed from Figs. 4 and 5 that the peak value of displacement response of type 1 increases as the power law exponent n increases. This can be explained as follows. Type 1 holds silicon nitride material properties on the inner surface and stainless-steel material properties on the outer surface. Small values of n correspond to a large volume fraction of stainless steel, whereas large values

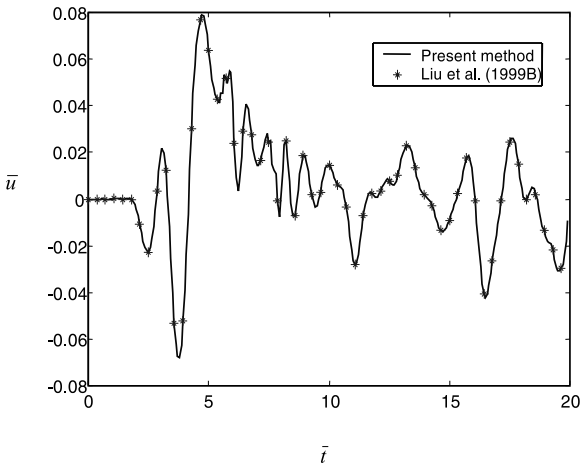

Fig. 2. The time history of the displacement at $x = 5H$ on the upper surface on the SiC–C FGM plate excited by an incident wave of one cycle of sine function at $x = 0$.

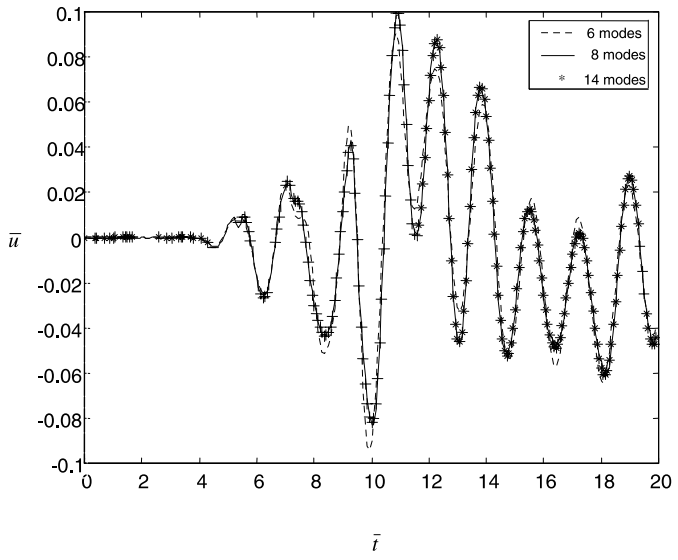

Fig. 3. A comparison of displacement responses at $x = 10H$ on the outer surface of type 1 cylindrical shell ($n = 2.0$) excited by an incident wave at $\bar{x} = 0$.

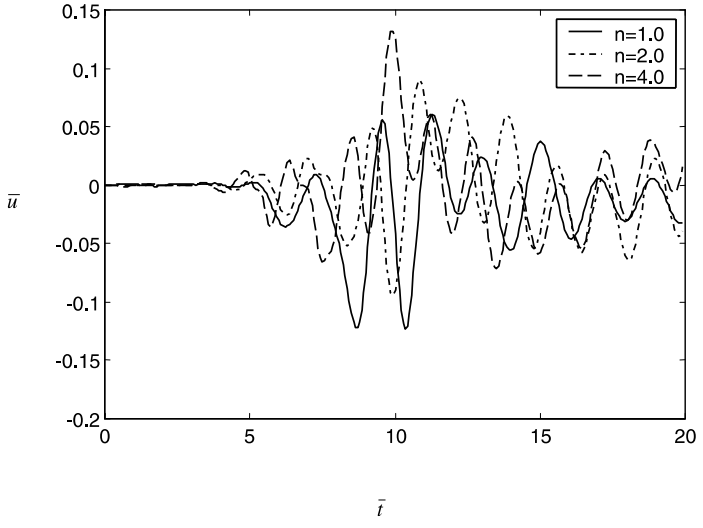

Fig. 4. Time history of the displacement at $x = 10H$ on the outer surface of type 1 cylinder ($R_1 = H$) excited by an incident wave at $x = 0$.

of n correspond to a large volume fraction of silicon nitride as shown in Eq. (42). The peak value of the displacement is $\bar{u}_{\max\,(\text{thick})} = 0.1318$ in Fig. 4 and it is $\bar{u}_{\max\,(\text{thin})} = 0.008838$ in Fig. 5. We can calculate the ratio:

$$\text{ratio} = \frac{\bar{u}_{\max\,(\text{thin})}}{\bar{u}_{\max\,(\text{thick})}} = \frac{0.008838 \times 21}{0.1318 \times 2} = 0.704. \tag{50}$$

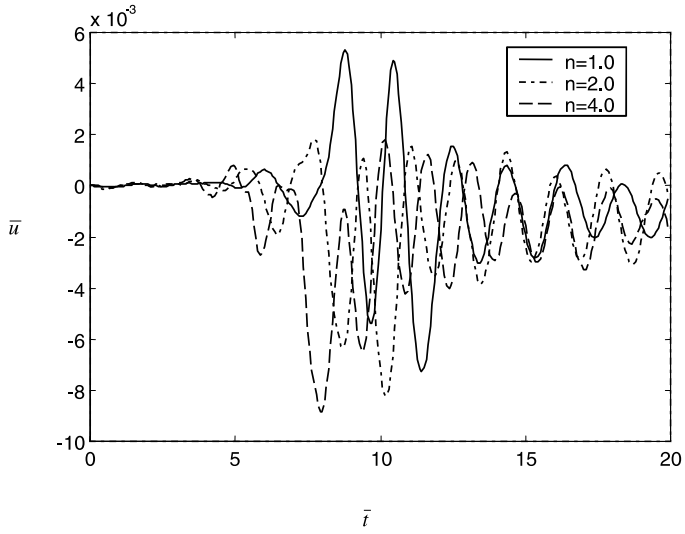

Fig. 5. Time history of the displacement at $x = 10H$ on the outer surface of type 1 cylindrical shell ($R_1 = 20H$) excited by an incident wave at $x = 0$.

It can be found that the peak value of the displacement response in cylindrical shell is less than that for cylinder.

Figs. 6 and 7 show the time history of the displacement $\bar{u}$ on the outer surface of the type 2 for thick cylinder and cylindrical shell, respectively. A comparison of the displacement response between various values of the power law exponent n is presented. It is obvious that the constituent volume fraction of type 2 is opposite to that of type 1, and thus, the power law exponent n influences conversely the displacement response of type 2. This can be explained as follows. Type 2 holds silicon nitride material properties on the outer surface and stainless-steel material properties on the inner surface. Large values of n correspond to a

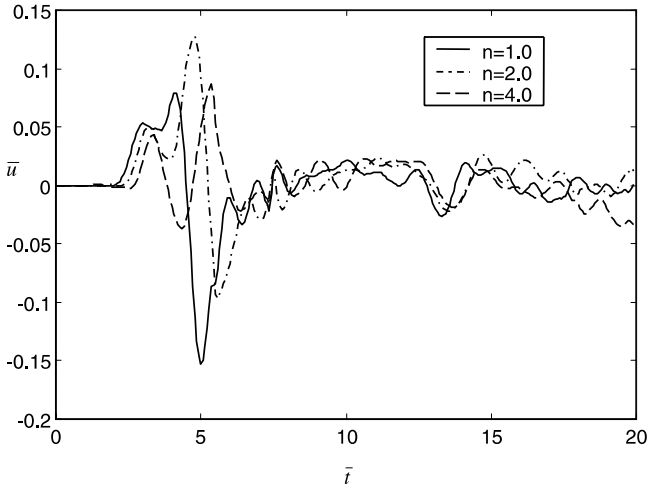

Fig. 6. Time history of the displacement at $x = 5H$ on the outer surface of type 2 cylinder ($R_1 = H$) excited by an incident wave at $x = 0$.

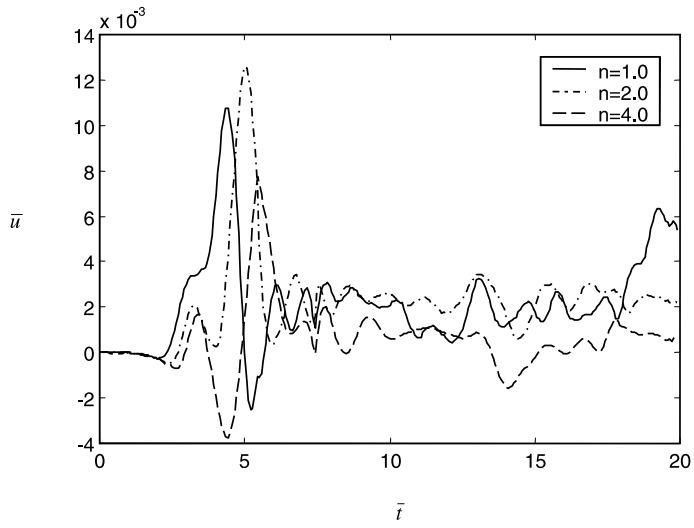

Fig. 7. Time history of the displacement at $x = 5H$ on the outer surface of type 2 cylindrical shell ($R_1 = 20H$) excited by an incident wave at $x = 0$.

large volume fraction of stainless steel, whereas small values of n correspond to a large volume fraction of silicon nitride as shown in Eq. (42).

Figs. 8 and 9 show the time history of displacement response on the outer surface of type 3 cylinder and cylindrical shell for the different constituent volume fraction varying with the power law exponent n, respectively. Comparing Figs. 8 and 9 with Figs. 4 and 5, it can be easily found that the variation of the displacement response with the value of n for type 3 is somewhat similar to that for type 1. The slight difference between the displacement response of types 1 and 3 is that the peak value of the response of type

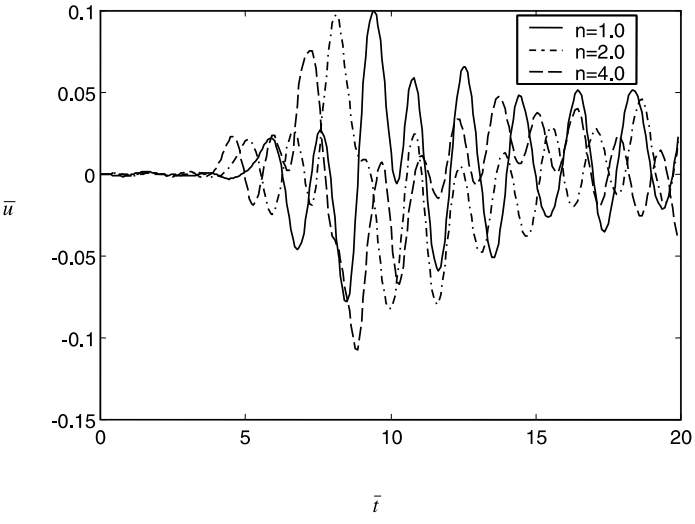

Fig. 8. Time history of the displacement at $x = 10H$ on the outer surface of type 3 cylinder ($R_1 = H$) excited by an incident wave at $x = 0$.

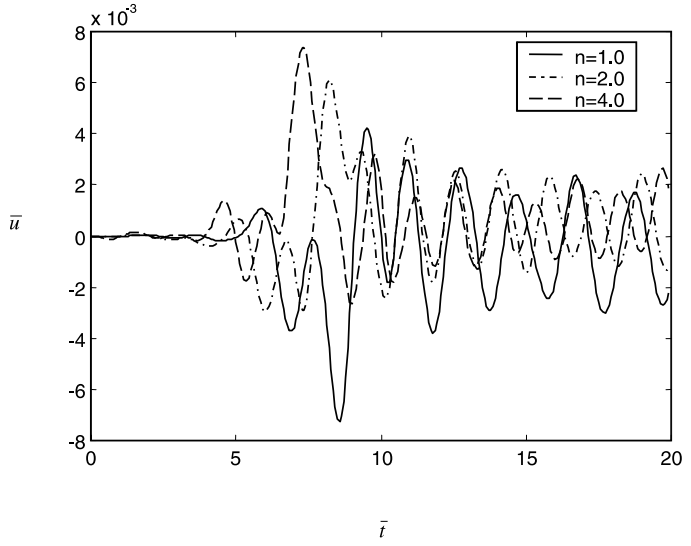

Fig. 9. Time history of the displacement at $x = 10H$ on the outer surface of type 3 cylindrical shell ($R_1 = 20H$) excited by an incident wave at $x = 0$.

3 is less than that of type 1 from comparing Figs. 4 and 8. In this case, the peak value of type 3 cylinder is $\bar{u}_{\max\,(\text{type }3)} = 0.1071$ and less than the peak value of type 1 cylinder which is $\bar{u}_{\max\,(\text{type }1)} = 0.1318$. Figs. 10 and 11 show the time history of displacement response on the outer surface of type 4 cylinder and cylindrical shell for the different constituent volume fraction varying with the power law exponent n, respectively. From these results, it can be found that the type 3 and 4 have better properties for attenuation of the displacement response induced by the same source of excitation.

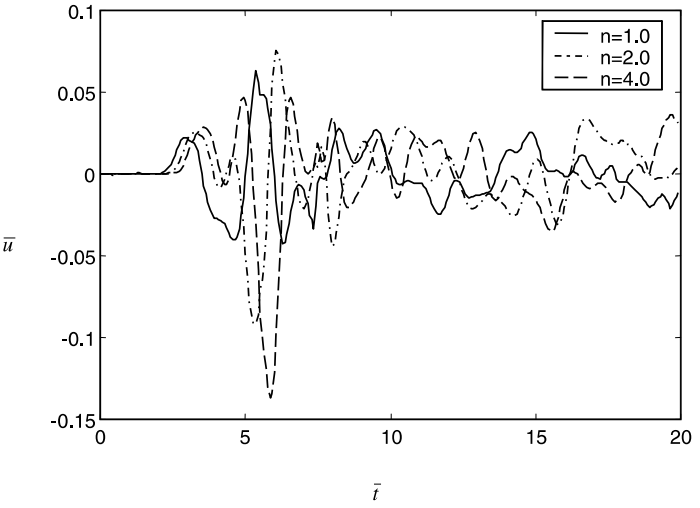

Fig. 10. Time history of the displacement at $x = 5H$ on the outer surface of type 4 cylinder ($R_1 = H$) excited by an incident wave at $x = 0$.

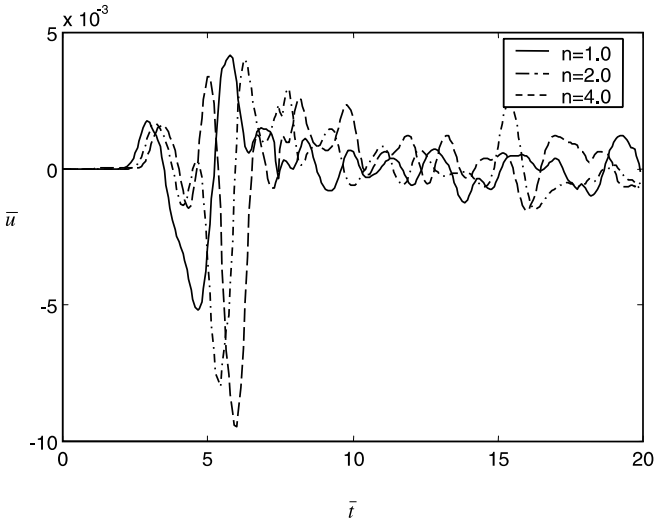

Fig. 11. Time history of the displacement at $x = 5H$ on the outer surface of type 4 cylindrical shell ($R_1 = 20H$) excited by an incident wave at $x = 0$.

5. Conclusions

HNM is presented for analyzing the displacement response of FGM cylinder excited by transient sources. This method combines the finite element method with the method of Fourier transforms. The material properties of each element are assumed to vary in the thickness direction, and it can give more accurate results for FGM. Moreover, this method reduces the spatial dimensions of the original problem by 1. As it adopts unidirectional nodal line numbering, it yields the minimum matrix bandwidth and requires much less computer memory and time.

Four types of FGM cylinders composed of stainless steel and silicon nitride are taken into account in this paper, and both cylinder and cylindrical shell are also studied. The results show that the peak value of displacement response on the outer surface in x axial of types 1, 3 and 4 increases as the power law exponent increases, and the peak value of displacement response is smaller of thin cylindrical shell. Type 3 and 4 FGM cylinder have better property for attenuation of the displacement response induced by the same stress source of excitation.

Appendix

$$\mathbf{A}_0^{\mathrm{d}} = \begin{bmatrix} (\frac{1}{5}h_n + \frac{1}{2}r_n)\mathbf{D}'_3 & (-\frac{2}{5}h_n - \frac{2}{3}r_n)\mathbf{D}'_3 & (\frac{1}{5}h_n + \frac{1}{6}r_n)\mathbf{D}'_3 \\ & (\frac{32}{15}h_n + \frac{8}{3}r_n)\mathbf{D}'_3 & (-\frac{26}{15}h - 2r_n)\mathbf{D}'_3 \\ \text{sym} & & (\frac{23}{15}h + \frac{11}{6}r_n)\mathbf{D}'_3 \end{bmatrix},$$

$$+\frac{h_n}{30}\begin{bmatrix} -4\mathbf{D}'_5 & 2\mathbf{D}'_5 & 1\mathbf{D}'_5 \\ -6 & -16\mathbf{D}'_5 & -2\mathbf{D}'_5 \\ \text{sym} & & 13\mathbf{D}'_5 \end{bmatrix} + \frac{1}{60h_n^4}\begin{bmatrix} c'_{11}\mathbf{D}'_6 & c'_{12}\mathbf{D}'_6 & c'_{13}\mathbf{D}'_6 \\ & c'_{22}\mathbf{D}'_6 & c'_{23}\mathbf{D}'_6 \\ \text{sym} & & c'_{33}\mathbf{D}'_6 \end{bmatrix},$$

where

$$\mathbf{D}_3' = \frac{1}{h_n}\mathbf{L}_2^{\mathrm{T}}[c_n^{\mathrm{O}} - c_n^{\mathrm{I}}]\mathbf{L}_2 = \frac{1}{h_n}\begin{bmatrix} \Delta c_{55}^n & 0 \\ 0 & \Delta c_{33}^n \end{bmatrix},$$

$$\mathbf{D}_5' = \frac{1}{2h_n}(\mathbf{L}_2^{\mathrm{T}}[c_n^{\mathrm{O}} - c_n^{\mathrm{I}}]\mathbf{L}_3 + \mathbf{L}_3^{\mathrm{T}}[c_n^{\mathrm{O}} - c_n^{\mathrm{I}}]\mathbf{L}_2) = \frac{1}{h_n}\begin{bmatrix} 0 & 0 \\ 0 & \Delta c_{23}^n \end{bmatrix},$$

$$\mathbf{D}_6' = \frac{1}{h_n}\mathbf{L}_3^{\mathrm{T}}[c_n^{\mathrm{O}} - c_n^{\mathrm{I}}]\mathbf{L}_3 = \frac{1}{h_n}\begin{bmatrix} 0 & 0 \\ 0 & \Delta c_{22}^n \end{bmatrix}$$

and

$$\begin{aligned} c_{11}' = {} & 2[4h_n^5 + 75h_n^4 r_n + 250r_n^2 h_n^3 + 300r_n^3 h_n^2 + 120r_n^4 h_n - 30r\ln(r_n + h_n)h_n^4 \\ & - 180r_n^2\ln(h_n + r_n)h_n^3 - 390r_n^3\ln(h_n + r_n)h_n^2 - 360r_n^4\ln(h_n + r_n)h_n - 120r_n^5\ln(r_n + h_n) \\ & + 180r_n^2\ln(r_n)h_n^3 + 30r_n\ln(r_n)h_n^4 + 360r_n^4\ln(r_n)h_n + 390r_n^3\ln(r_n)h_n^2 + 120r_n^5\ln(r_n)], \\ c_{12}' = {} & 4[h_n^5 - 10h_n^4 r_n - 130r_n^2 h_n^3 - 240r_n^3 h_n^2 - 120r_n^4 h_n \\ & + 60r_n^2\ln(h_n + r_n)h_n^3 + 240r_n^3\ln(h_n + r_n)h_n^2 + 300r_n^4\ln(h_n + r_n)h_n + 120r_n^5\ln(r_n + h_n) \\ & - 60r_n^2\ln(r_n)h_n^3 - 300r_n^4\ln(r_n)h_n - 240r_n^3\ln(r_n)h_n^2 - 120r_n^5\ln(r_n)], \\ c_{13}' = {} & -2[h_n^5 - 5h_n^4 r_n - 70r_n^2 h_n^3 - 180r_n^3 h_n^2 - 120r_n^4 h_n + 30r_n^2\ln(h_n + r_n)h_n^3 + 150r_n^3\ln(h_n + r_n)h_n^2 \\ & + 240r_n^4\ln(h_n + r_n)h_n + 120r_n^5\ln(r_n + h_n) - 30r_n^2\ln(r_n)h_n^3 - 240r_n^4\ln(r_n)h_n \\ & - 150r_n^3\ln(r_n)h_n^2 - 120r_n^5\ln(r_n)], \\ c_{22}' = {} & 16[2h_n^5 - 5h_n^4 r_n + 20r_n^2 h_n^3 + 90r_n^3 h_n^2 + 60r_n^4 h_n - 60r_n^3\ln(h_n + r_n)h_n^2 - 120r_n^4\ln(h_n + r_n)h_n \\ & - 60r_n^5\ln(r_n + h_n) + 120r_n^4\ln(r_n)h_n + 60r_n^3\ln(r_n)h_n^2 + 60r_n^5\ln(r_n)], \\ c_{23}' = {} & 4[h_n^5 - 120h_n^4 r_n - 10r_n^2 h_n^3 - 120r_n^3 h_n^2 + 60r_n^3\ln(h_n + r_n)h_n^2 + 180r_n^4\ln(h_n + r_n)h_n + 120r_n^5\ln(r_n + h_n) \\ & - 180r_n^4\ln(r_n)h_n - 60r_n^3\ln(r_n)h_n^2 - 120r_n^5\ln(r_n)], \\ c_{33}' = {} & 2[4h_n^5 - 5h_n^4 r_n + 10r_n^2 h_n^3 + 60r_n^3 h_n^2 + 120r_n^4 h_n - 30r_n^3\ln(h_n + r_n)h_n - 120r_n^4\ln(h_n + r_n)h_n \\ & - 120r_n^5\ln(r_n + h_n) + 120r_n^4\ln(r_n)h_n + 30r_n^3\ln(r_n)h_n^2 + 120r_n^5\ln(r_n)]. \end{aligned}$$

$$\begin{aligned} \mathbf{A}_1^{\mathrm{d}} = {} & \frac{h_n}{30}\begin{bmatrix} -(h_n + 4r_n)\mathbf{D}_2'' & -4(h_n + 3r_n)\mathbf{D}_2'' & (5h_n + 6r_n)\mathbf{D}_2'' \\ 4(h_n + 2r_n)\mathbf{D}_2'' & -16(h_n + r_n)\mathbf{D}_2'' & -4(7h_n + 8r_n)\mathbf{D}_2'' \\ -(3h_n + 4r_n)\mathbf{D}_2'' & 4(5h_n + 7r_n)\mathbf{D}_2'' & (23h_n + 26r_n)\mathbf{D}_2'' \end{bmatrix} \\ & + \frac{h_n}{30}\begin{bmatrix} (h_n + 4r_n)\mathbf{D}_2''' & 2r_n\mathbf{D}_2''' & (h_n + r_n)\mathbf{D}_2''' \\ & 16(h_n + r_n)\mathbf{D}_2''' & 2(2h_n + r_n)\mathbf{D}_2''' \\ \text{sym} & & -(23h_n + 26r_n)\mathbf{D}_2''' \end{bmatrix} \\ & + \frac{h_n^2}{30}\begin{bmatrix} \mathbf{D}_4'' - \mathbf{D}_4''' & 0 & \mathbf{D}_4''' - \mathbf{D}_4'' \\ & 16(\mathbf{D}_4'' - \mathbf{D}_4''') & 4(\mathbf{D}_4'' - \mathbf{D}_4''') \\ \text{sym} & & 7(\mathbf{D}_4'' - \mathbf{D}_4''') \end{bmatrix}, \end{aligned}$$

where

$$\mathbf{D}_2'' = \frac{1}{2h_n}(\mathbf{L}_1^{\mathrm{T}}[c_n^{\mathrm{O}} - c_n^{\mathrm{I}}]\mathbf{L}_2 + \mathbf{L}_2^{\mathrm{T}}[c_n^{\mathrm{O}} - c_n^{\mathrm{I}}]\mathbf{L}_1) = \frac{1}{2h_n}\begin{bmatrix} 0 & \Delta c_{13}^n + \Delta c_{15}^n \\ \Delta c_{13}^n + \Delta c_{15}^n & 0 \end{bmatrix},$$

$$\mathbf{D}_4'' = \frac{1}{2h_n}(\mathbf{L}_1^{\mathrm{T}}[c_n^{\mathrm{O}} - c_n^{\mathrm{I}}]\mathbf{L}_3 + \mathbf{L}_3^{\mathrm{T}}[c_n^{\mathrm{O}} - c_n^{\mathrm{I}}]\mathbf{L}_1) = \frac{1}{2h_n}\begin{bmatrix} 0 & \Delta c_{12}^n \\ \Delta c_{12}^n & 0 \end{bmatrix},$$

$$\mathbf{D}_2''' = \frac{1}{h_n}\mathbf{L}_1^{\mathrm{T}}[c_n^{\mathrm{O}} - c_n^{\mathrm{I}}]\mathbf{L}_2 = \frac{1}{h_n}\begin{bmatrix} 0 & \Delta c_{13}^n \\ \Delta c_{55}^n & 0 \end{bmatrix},$$

$$\mathbf{D}_4''' = \frac{1}{h_n}\mathbf{L}_1^{\mathrm{T}}[c_n^{\mathrm{O}} - c_n^{\mathrm{I}}]\mathbf{L}_3 = \frac{1}{h_n}\begin{bmatrix} 0 & \Delta c_{12}^n \\ 0 & 0 \end{bmatrix},$$

$$\mathbf{A}_2^{\mathrm{d}} = \frac{h_n^2}{420}\begin{bmatrix} (2h_n + 7r_n)\mathbf{D}_1' & -4h_n\mathbf{D}_1' & -(5h_n + 7r_n)\mathbf{D}_1' \\ & 16(4h_n + 7r_n)\mathbf{D}_1' & 4(6h_n + 7r_n)\mathbf{D}_1' \\ \text{sym} & & (44h_n + 49r_n)\mathbf{D}_1' \end{bmatrix},$$

where

$$\mathbf{D}_1' = \frac{1}{h_n}\mathbf{L}_1^{\mathrm{T}}[c_n^{\mathrm{O}} - c_n^{\mathrm{I}}]\mathbf{L}_1 = \frac{1}{h_n}\begin{bmatrix} \Delta c_{11}^n & 0 \\ 0 & \Delta c_{55}^n \end{bmatrix},$$

$$\mathbf{M}_{\mathrm{d}} = \frac{h_n\Delta\rho_n}{420}\begin{bmatrix} (2h_n + 7r_n)\mathbf{I} & -4h_n\mathbf{I} & -(5h_n + 7r_n)\mathbf{I} \\ & 16(4h_n + 7r_n)\mathbf{I} & 4(6h_n + 7r_n)\mathbf{I} \\ \text{sym} & & (44h_n + 49r_n)\mathbf{I} \end{bmatrix}.$$

References

Chou, F.H., Achenbach, J.D., 1981. Three-dimensional vibrations of orthotropic cylinders. ASCE Journal of Engineering Mechanics 98, 813–822.

Gong, S.W., Lam, K.Y., Reddy, J.N., 1999. The elastic response of functionally graded cylindrical shells to low-velocity impact. International Journal of Impact Engineering 22, 397–417.

Liu, G.R., Han, X., Lam, K.Y., 1999a. Stress waves in functionally gradient materials and its use for material characterization. Composite Part B 30, 383–394.

Liu, G.R., Han, X., Lam, K.Y., 1999b. Material Characterization of FGM plates using elastic waves and an inverse procedure. Journal of Composite Materials, submitted for publication.

Liu, G.R., Lam, K.Y., 1999c. Transient waves in a laminated composite plate to a point excitation. The proceedings of twelfth international conference on composite materials, Paris, July 5–9, Paper No. 1367.

Liu, G.R., Lam, K.Y., Ohyoshi, T., 1997. A technique for analyzing elastodynamic responses of anisotropic laminated plates to line loads. Composites Part B 28B, 667–677.

Liu, G.R., Lam, K.Y., Shang, H.M., 1995. A new method for analyzing wave fields in laminated composite plates: Two-dimensional cases. Composite Engineering 5 (12), 1489–1498.

Liu, G.R., Tani, J., 1994. Surface waves in functionally gradient piezoelectric plates. ASME Journal of vibration and acoustics 116, 440–448.

Liu, G.R., Tani, J., Ohyoshi, T., 1991a. Lamb waves in a functionally gradient material plates and its transient response. Part 1: Theory; Part 2: Calculation results. Transactions of the Japan Society of Mechanical Engineers 57A (535), 131–142.

Liu, G.R., Tani, J., Ohyoshi, T., Watanabe, K., 1991b. Transient waves in anisotropic laminated plates, part 1: Theory; Part 2. Applications Journal of vibration and acoustics 113, 230–239.

Liu, G.R., Tani, J., 1992. SH surface waves in functionally gradient piezoelectric material plates. Transactions of the Japan society of mechanical engineers 58A (547), 504–507.

Mirsky, I., 1964. Axisymmetric vibrations of orthotropic cylinders. Journal of the acoustical society of America 36 (11), 2106–2112.

Nayfeh, A.H., 1995. Wave propagation in layered anisotropic media with applications to composites. Elsevier, Amsterdam.

Nowinski, J.L., 1967. Propagation of longitudinal waves in circular cylindrical orthotropic bars. Journal of Engineering for Industry 89, 408–412.

Ohyoshi, T., Sui, G.J., Miuro, K., 1996. Using of stacking model of the linearly inhomogeneous layers elements. Proceedings of the ASME aerospace Division 52, 101–106.

Touloukian, Y.S., 1967. Thermophysical Properties of High Temperature Solid Materials. Macmillan, New York.

Xi, Z.C., Liu, G.R., Lam, K.Y., Shang, H.M., 1999. A strip element method for analyzing wave scattering by a crack in a laminated composite cylinder. ASME Journal of Applied Mechanics, submitted for publication.

Yuan, F.G., Hsieh, C.C., 1998. Three-dimensional wave propagation in composite cylindrical shells. Composite Structures 42, 153–167.